

## Tropical precipitation and convection changes in the Max Planck Institute Earth system model (MPI-ESM) in response to CO<sub>2</sub> forcing

Traute Crueger,<sup>1</sup> Cathy Hohenegger,<sup>1</sup> and Wilhelm May<sup>2</sup>

Received 27 July 2012; revised 1 November 2012; accepted 4 January 2013; published 6 March 2013.

[1] In this study, the sensitivity of tropical precipitation and convection to CO<sub>2</sub> forcing is examined. In order to test the robustness of the response, two simulations with idealized CO<sub>2</sub> forcings following CMIP5, one with a smooth and one with an abrupt CO<sub>2</sub> increase, are analyzed. The simulations are performed with the Max Planck Institute Earth system model (MPI-ESM). Beyond investigating the mean precipitation response, high-frequency (30 min) direct output of the convection scheme is considered to better assess the ability of the convection scheme to reproduce results from cloud-resolving simulations or physical argumentation. Over the tropics, precipitation increases by 1.7% K<sup>-1</sup> almost independently of the CO<sub>2</sub> forcing. Over land, the response under transient CO<sub>2</sub> forcing is also positive, but negative under an abrupt CO<sub>2</sub> increase. In both cases precipitation tends to follow evaporation, but the latter reacts differently due to land surface processes. The Madden-Julian oscillation also shows different sensitivities for the two CO<sub>2</sub> forced climates. As the climate warms, deep convection gets more intense, less frequent, and deeper. The cloud top temperatures remain constant, whereas cumulus congestus and shallow clouds warm. As such, the MPI-ESM and its convection scheme hold for the fixed-anvil temperature hypothesis. This implies an enhancement of the deep convective cloud height by 3–4% K<sup>-1</sup>. Changes in precipitation intensity and convective cloud base properties scale with the Clausius-Clapeyron equation, whereas the energy constraint determines changes in precipitation frequency. This is true over the tropics considered as a whole and over the tropical oceans, but breaks down over land.

**Citation:** Crueger, T., C. Hohenegger, and W. May, Tropical precipitation and convection changes in the Max Planck Institute Earth system model (MPI-ESM) in response to CO<sub>2</sub> forcing, *J. Adv. Model. Earth Syst.*, 5, 85–97, doi:10.1002/jame.20012.

### 1. Introduction

[2] The hydrological cycle of the Earth is of particular interest with respect to climate change. One important aspect concerns precipitation changes in the tropics, which are tightly tied to changes in convection, specifically deep convection. Tropical clouds have large impacts on the radiation budget and hence on climate sensitivity in response to an increase of CO<sub>2</sub> [Bony and Dufresne, 2005]. Deep convection acts as a fundamental source of heat in the middle troposphere via vertical latent heat transport from the surface and is thus a driver of the global circulation. The most dominant mode of tropical intraseasonal variability, the Madden-Julian oscillation (MJO), is also strongly linked to deep convection [Zhang, 2005]. Therefore, changes in tropi-

cal precipitation and convection in response to atmospheric CO<sub>2</sub> increase are of fundamental regional and global importance.

[3] Analysis of climate projections has generally revealed that the hydrological cycle intensifies as the climate warms [Intergovernmental Panel on Climate Change (IPCC) 2007, Allen and Ingram, 2002; Andrews and Forster, 2010]. According to such projections, tropical precipitation mainly increases over the Equatorial Pacific and Indian Ocean, whereas reductions have been primarily obtained over the land areas of Amazonia and Australia [IPCC, 2007]. Besides scenario experiments, experiments driven by idealized CO<sub>2</sub> forcing are useful, because they allow an easier interpretation of some aspects of the climate change signal and an isolation of feedback processes acting on different time scales [e.g., Knutson and Manabe, 1995; Yang et al., 2003; Gregory and Webb, 2008; Andrews and Forster, 2010].

[4] Despite large uncertainties in the precipitation response obtained by different climate models on local scales, some robust responses of the hydrological cycle have been isolated. Held and Soden [2006] examined

<sup>1</sup>Max Planck Institute for Meteorology, Hamburg, Germany.

<sup>2</sup>Danish Meteorological Institute, Copenhagen, Denmark.

model data of the AR4 archive and found a robust increase of global precipitation for the different models, on the order of 2% per degree temperature warming. This is substantially lower than the increase of water vapor saturation of  $7\% \text{ K}^{-1}$  predicted by the Clausius-Clapeyron equation but is consistent with the idea that global precipitation is constrained by the global energy budget [see also e.g., *Allen and Ingram, 2002*]. *Held and Soden [2006]* concluded that the strengthening of the hydrological cycle implies a decrease of the mass flux between the boundary layer and the midtroposphere. Furthermore, they argued that this mass flux mainly occurs via moist convection in the tropics and thus suggested a change in tropical convection accompanying global warming. Changes in tropical precipitation have also been examined by *Romps [2011]* using high-resolution cloud-resolving simulations with explicit convection. *Romps [2011]* found a general trend toward higher tropical precipitation fluxes with increasing  $\text{CO}_2$ . In addition, he showed that the most intense precipitation events are produced by deep convective clouds that are larger and wider, but less frequent. For tropical deep convective clouds, *Hartmann and Larsson [2002]* suggested that the temperature at which the anvils detrain remains constant despite climate change based on an analysis of radiative-convective equilibrium simulations. This so-called fixed-anvil temperature (FAT) hypothesis implies that the cloud top height rises as the troposphere warms. The FAT hypothesis has been confirmed by *Kuang and Hartmann [2007]* in a three-dimensional cloud-resolving model and indirectly in global climate model simulations by noting an upward shift of the mean atmospheric profile with global warming [e.g., *Wright et al., 2010; Satoh et al., 2012*].

[5] In this study, the response of tropical precipitation and convection to idealized  $\text{CO}_2$  forcings is examined using the fully coupled Max Planck Institute Earth system model (MPI-ESM). The newest release, specifically developed for the intercomparison exercise CMIP5, is employed. The specific goal of this study is to investigate the robustness of the precipitation change signal. When we speak of robustness in this article, we refer to the precipitation response over land versus ocean, the precipitation response to different pathways of  $\text{CO}_2$  forcing (smooth versus abrupt), and the strength of the intraseasonal MJO and its sensitivity to the different  $\text{CO}_2$  pathways. Finally, we assess the ability of the convection scheme to reproduce precipitation changes as expected from physical argumentation and/or cloud-resolving studies using explicit convection. The two  $\text{CO}_2$  forcings considered are one simulation with a continuous  $\text{CO}_2$  increase of 1% per year with respect to preindustrial level, and one with an abrupt 4 times  $\text{CO}_2$  concentration increase, in accordance with the CMIP5 protocol [see *Taylor et al., 2012*]. As for the rules governing precipitation changes, the Clausius-Clapeyron scaling, the energy budget constraint and the FAT hypothesis are considered here.

[6] The study positions itself in the wealth of previous studies which have investigated precipitation changes in response to different forcings/scenarios, albeit conducted

here under the CMIP5 umbrella and employing the latest version of the MPI-ESM. Although the model represents the most up-to-date representation of the climate system, large biases still exist in the simulation of present-day precipitation [see e.g., *Stevens et al., 2013*]. Parts of these biases are attributable to the convection scheme. Hence, special emphasis is placed on the analysis of changes in convection statistics directly derived from the convection scheme. In contrast to previous studies, direct outputs from the convection scheme are saved every other time step (i.e., every 30 min) for specific years. This approach also allows a more direct testing of climate change rules.

[7] The outline of the paper is as follows: First an overview of temperature and precipitation changes is given for different regions and the two  $\text{CO}_2$  experiments. Changes in the MJO are then examined, followed by the changes in convection statistics. Finally, the precipitation response is assessed, with special focus on the extent to which the MPI-ESM and its convection scheme can reproduce the three climate change rules mentioned previously.

## 2. Methods

### 2.1. Model

[8] The MPI-ESM is the new version of the coupled model of the Max Planck Institute for Meteorology. It consists of the atmosphere model ECHAM6 [*Stevens et al., 2013*], including the land and vegetation module JSBACH (C. H. Reick et al., The representation of natural and anthropogenic land cover change in MPI-ESM, submitted to *Journal of Advances in Modeling Earth Systems*, 2012) and the ocean model MPIOM (J. Jungclaus et al., Characteristics of the ocean simulations in MPIOM, the ocean component of the MPI-Earth System Model, submitted to *Journal of Advances in Modeling Earth Systems*, 2012), including the module for marine biogeochemistry HAMOCC5 [*Ilyina et al., 2013*]. One of the main differences between ECHAM6 and its predecessor ECHAM5 is that ECHAM6 is run at a higher vertical resolution, i.e., 47 instead of 31 vertical levels, which leads to a better representation of the upper troposphere/stratosphere. Furthermore, ECHAM6 incorporates a completely new aerosol climatology (S. Kinne et al., A new global aerosol climatology for climate studies, submitted to *Journal of Advances in Modeling Earth Systems*, 2012) and uses a new shortwave radiation scheme that has less cloud absorption [*Stevens et al., 2013*]. As in ECHAM5, the convection scheme is the Tiedtke scheme with Nordeng's modifications of deep convection [*Tiedtke, 1989; Nordeng, 1994; B. Möbis, and B. Stevens, Mechanisms controlling the ITCZ placement in idealized simulations with ECHAM6, submitted to Journal of Advances in Modeling Earth Systems, 2012*].

### 2.2. Experiments

[9] The experiments examined in this study are conducted according to the CMIP5 protocol [*Taylor et al., 2012*]. They are performed under two idealized  $\text{CO}_2$  forcings. The first experiment, denoted in the following as 1pct $\text{CO}_2$ , experiences a  $\text{CO}_2$  increase of 1% per year,

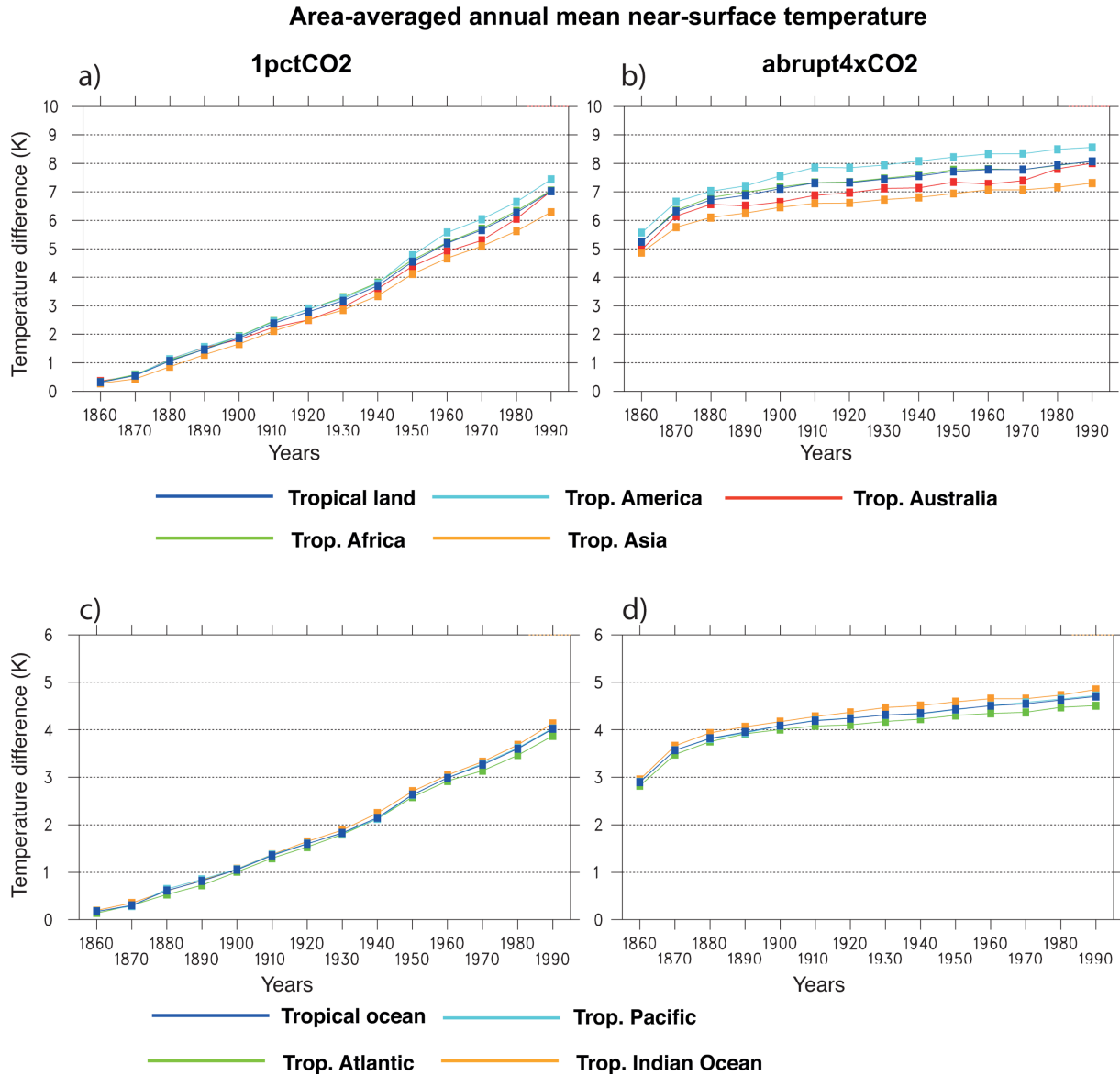


**Figure 1.** Changes in annual mean near-surface temperature (K) with respect to piControl for 14 20-year periods for (a, c) 1pctCO<sub>2</sub> and (b, d) abrupt4×CO<sub>2</sub> averaged over different (a, b) land and (c, d) oceanic regions. The areas considered are the tropical parts of four continents and three ocean basins. The tropical Pacific curve is hidden behind the tropical ocean curve. The band between 26° S and 26° N defines the tropics.

beginning at a preindustrial atmospheric CO<sub>2</sub> concentration. In the second one, an abrupt CO<sub>2</sub> increase of four times its preindustrial concentration is imposed at the initial time (year 1850) and kept constant throughout the experiment (1140 ppm). This experiment is referred to as abrupt4×CO<sub>2</sub>. Both simulations are performed for 150 years. At the end of the 150 years, CO<sub>2</sub> concentrations in 1pctCO<sub>2</sub> and abrupt4×CO<sub>2</sub> are roughly similar (abrupt4×CO<sub>2</sub>: 1140 ppm, 1pctCO<sub>2</sub>: 1130 ppm (1990), 1250 ppm (1999)). As a reference simulation, a 150 year period of the preindustrial control simulation with a fixed CO<sub>2</sub> concentration of 285 ppm is utilized, which is referred to as piControl. For the

analysis of these simulations, focus is set on the tropical belt from 26°S to 26°N.

### 3. Results

#### 3.1. Surface Temperature

[10] Figure 1 shows changes in temperature with time for 1pctCO<sub>2</sub> and abrupt4×CO<sub>2</sub> (with respect to piControl) averaged over different regions. The two simulations reveal different rates of temperature change in response to the differently increasing CO<sub>2</sub> concentrations. However, the land and ocean areas behave similarly in this respect: In 1pctCO<sub>2</sub>, there is an almost steadily linear

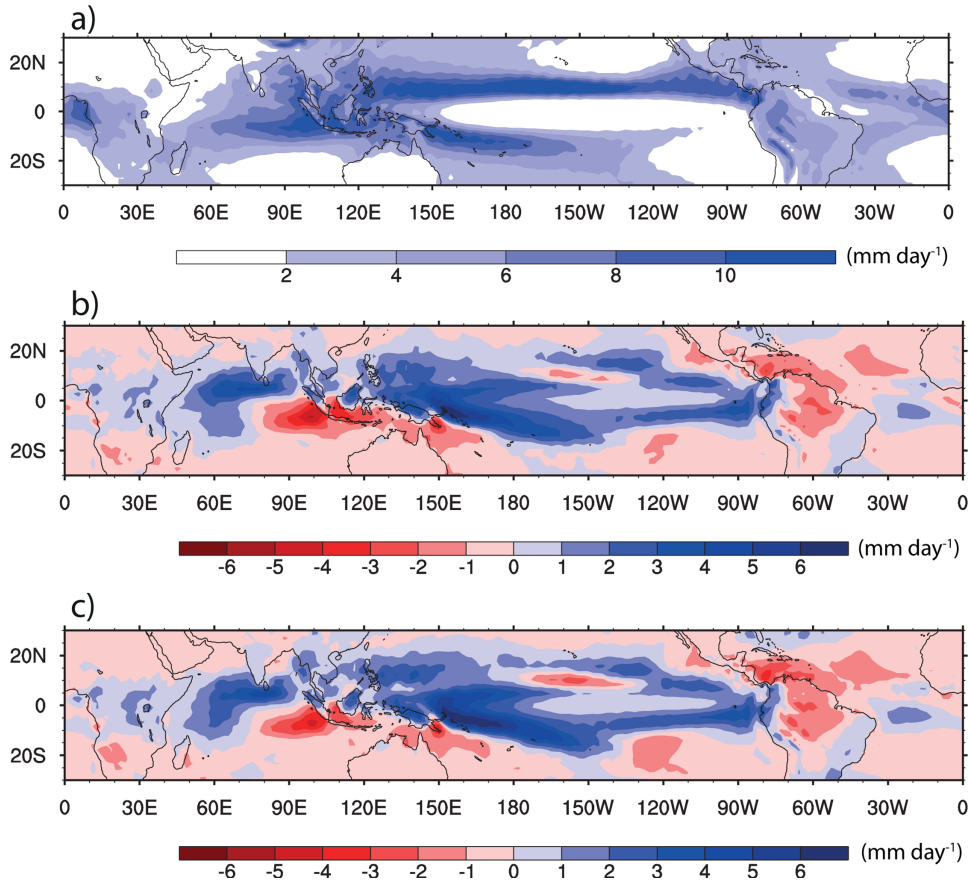


**Figure 2.** (a) Annual mean daily precipitation for 20 years of piControl. The lower two panels show changes in annual mean daily precipitation for (b) 1pctCO<sub>2</sub> and (c) abrupt4×CO<sub>2</sub> with respect to piControl averaged over the years 1990–1999. Units are (mm d<sup>-1</sup>).

temperature increase. In abrupt4×CO<sub>2</sub>, after an abrupt increase, temperature only rises slowly. About two thirds of the total temperature response occurs abruptly over land and ocean in abrupt4×CO<sub>2</sub>. Generally, the land temperatures, with an increase of 7 K in 1pctCO<sub>2</sub> and 8 K in abrupt4×CO<sub>2</sub> after 150 years, rise more strongly than over the ocean areas, where the increase only amounts to 4 K in 1pctCO<sub>2</sub> and nearly 5 K in abrupt4×CO<sub>2</sub>. Tropical America in abrupt4×CO<sub>2</sub> experiences the strongest warming (8.5 K), while tropical Asia exhibits the smallest temperature increase among the tropical land areas (7 K). With respect to the ocean basins, the increase is smallest over the tropical Atlantic (4.5 K) and largest over the Indian Ocean (4.8 K). The stronger warming over land is qualitatively consistent with previous findings from e.g., multimodel means performed with the SRES A1B scenario [IPCC, 2007; Sutton *et al.*, 2007] and appears to be independent of the forcing mechanism. According to Dong *et al.* [2009] and Joshi *et al.* [2008], the reasons for the stronger warming over land are related to local feedbacks and hydrologic processes over land.

[11] After 150 years, abrupt4×CO<sub>2</sub> has not fully attained equilibrium yet. The temperatures are also 1 K warmer over land and 0.5 K warmer over ocean than in 1pctCO<sub>2</sub>, although both simulations have reached simi-

lar CO<sub>2</sub> concentrations. Despite this, the temperature signal may be seen as mostly robust in the sense that ranking the regions according to the strength of the experienced warming yields the same result in 1pctCO<sub>2</sub> and abrupt4×CO<sub>2</sub>. The ranking seems already set in the first year in abrupt4×CO<sub>2</sub>, suggesting similar signs of the fast and slow atmospheric responses to the imposed CO<sub>2</sub> radiative forcing.

### 3.2. Precipitation

[12] The precipitation response to the CO<sub>2</sub> forcing for the last decade of both simulations is illustrated in Figure 2. The precipitation change signal exhibits a similar structure in the two simulations, characterized by a ring-like structure of enhanced precipitation over the Pacific with a strong increase over its western part, reduced precipitation over parts of the Warm Pool area and Amazonia, and a dipole structure over the Indian Ocean (Figures 2b and 2c). It is noteworthy that, even after the first simulation decade, 1pctCO<sub>2</sub> and abrupt4×CO<sub>2</sub> show a similar geographical distribution of the precipitation changes as after the last simulation decade, even though the magnitudes may differ (not shown).

[13] The precipitation increase in the west Equatorial Pacific amounts up to 50%, although this area is even a

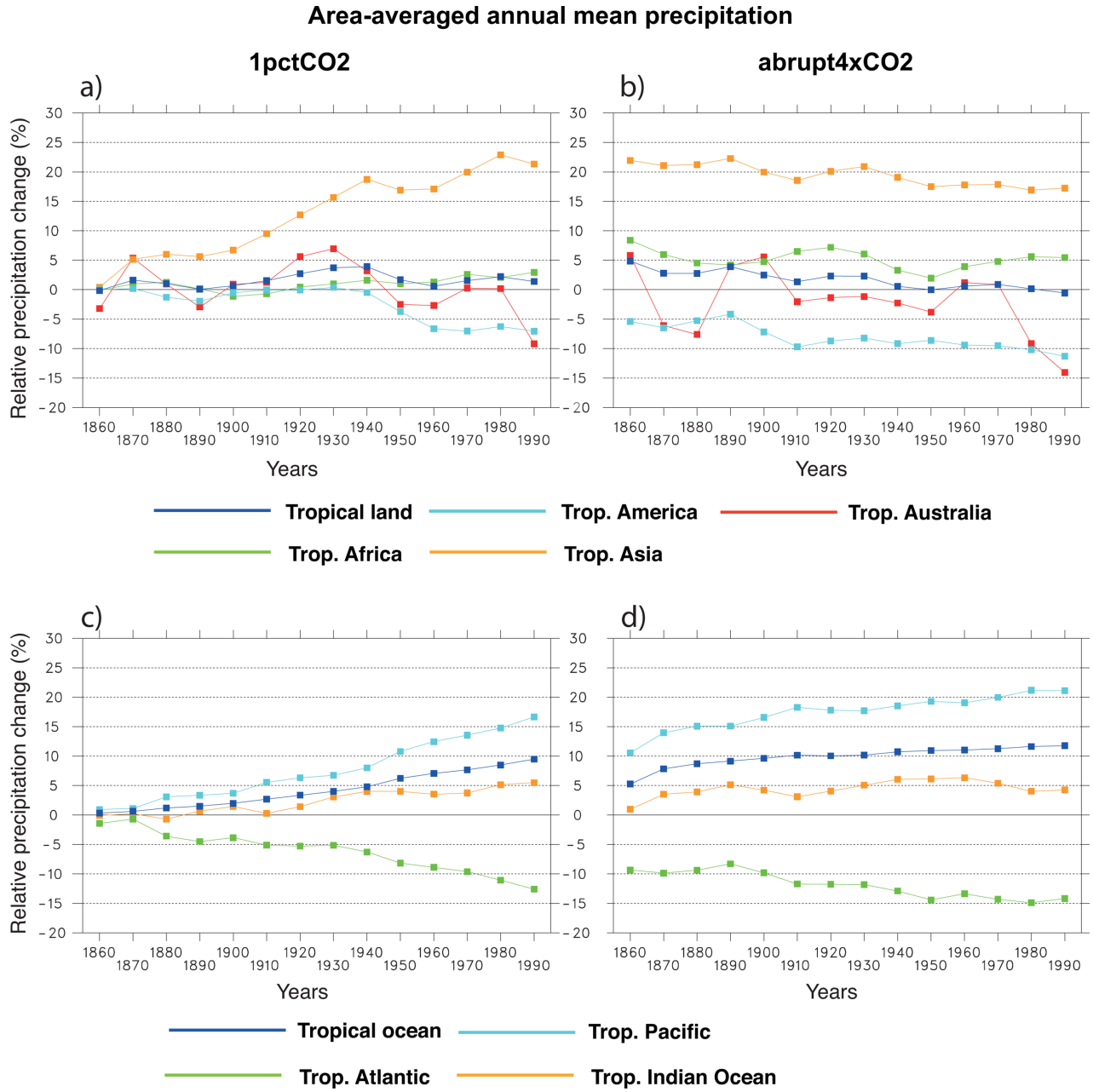


**Figure 3.** Same as Figure 1 but for the relative changes (%) in the area mean annual precipitation.

high precipitation area in piControl (Figure 2a). The increase is especially obvious south of the Equator up to the north-western South American coast. Here the changes north and south of the equator seem to reflect a northward shift of the Intertropical Convergence Zone (ITCZ). Precipitation increases by more than  $3 \text{ mm d}^{-1}$  south of India, which implies more than a doubling of precipitation. On the other hand, the belt of decreased precipitation simulated southwest and southeast of the Indonesian islands, up to northern Australia and the Pacific, means a rainfall reduction of up to 25%. Concerning the land areas, most of the islands in the Warm Pool region show increased precipitation, about 25%. A considerable precipitation decrease of

20% is found over Amazonia whereas the remaining land areas exhibit small changes. These results marked by strongest increases over the Warm Pool, the Equatorial Pacific, and the Indian Ocean south of India are in line with those reported for instance in the IPCC report [IPCC, 2007] for the SRES A1B scenario and the multi-model ENSEMBLES experiment [Johns *et al.*, 2011]. Also, the precipitation decreases, especially in the Indian Ocean basin northwest of Australia, are consistent with the IPCC multimodel results.

[14] Although the precipitation change patterns have similar structures in 1pctCO<sub>2</sub> and abrupt4×CO<sub>2</sub>, consideration of the relative precipitation changes for different ocean basins and landmasses as a function of

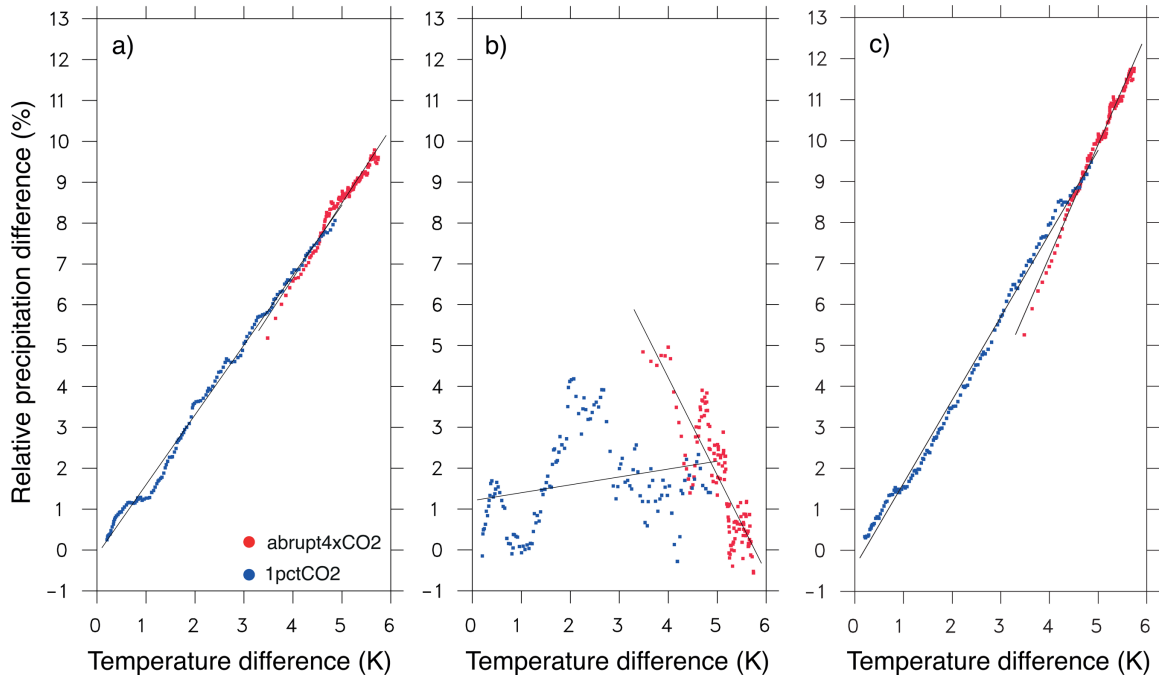


**Figure 4.** Relative changes (%) in area mean annual precipitation with respect to piControl for 1pctCO<sub>2</sub> (blue) and abrupt4×CO<sub>2</sub> (red) as a function of the corresponding changes in the globally averaged annual mean near-surface temperature (K). The areas considered are (a) the tropics, (b) the tropical landmasses, and (c) the tropical oceans. The black lines indicate the regression lines. The slopes for 1pctCO<sub>2</sub> are 1.7% K<sup>-1</sup> in Figure 4a, 0.2% K<sup>-1</sup> in Figure 4b, and 2.0% K<sup>-1</sup> in Figure 4c. The corresponding slopes for abrupt4×CO<sub>2</sub> are 1.8% K<sup>-1</sup>, -2.4% K<sup>-1</sup>, and 2.7% K<sup>-1</sup>.

time reveals different pathways (Figure 3). While for 1pctCO<sub>2</sub> changes are negligible in the first 20 experiment years, abrupt4×CO<sub>2</sub> reveals an abrupt and strikingly high change in precipitation even in this period. There is also a tendency in abrupt4×CO<sub>2</sub> over the tropical land area for precipitation to abruptly increase followed by a weak decrease. In contrast, precipitation tends to continuously increase in 1pctCO<sub>2</sub> except over tropical Australia and tropical America. Differences between 1pctCO<sub>2</sub> and abrupt4×CO<sub>2</sub> are especially pronounced over tropical Asia. Tropical Asia shows an abrupt increase of about 22% in abrupt4×CO<sub>2</sub>, which then reduces to 17% compared to piControl. In 1pctCO<sub>2</sub>, the Asian rainfall increases steadily to a change of more than 20%. All land areas end up with a surplus of precipitation except for tropical Australia and America. The overall precipitation reduction amounts to 10% (1pctCO<sub>2</sub>) and 14% (abrupt4×CO<sub>2</sub>) for tropical Australia and to 7% (1pctCO<sub>2</sub>) and 11% (abrupt4×CO<sub>2</sub>) for tropical America, but with considerable temporal variability.

[15] In contrast to the land areas, the temporal evolution of the oceanic precipitation changes in abrupt4×CO<sub>2</sub> resembles the evolution in 1pctCO<sub>2</sub>. Both simulations show continuous increase or continuous decrease over the same basins, although the rates of change are distinct. The global tropical oceans show a precipitation increase of 9% in 1pctCO<sub>2</sub> and 12% in

abrupt4×CO<sub>2</sub>. As apparent in Figure 3, the largest changes are over the tropical Pacific with a rainfall increase of 20%. The opposite is the case for the tropical Atlantic which obtains considerable less rainfall as compared to piControl (15% reduction). Consistent with temperature, ranking the regions per strength of the resulting precipitation change yields similar results in 1pctCO<sub>2</sub> and abrupt4×CO<sub>2</sub>.

[16] Figure 4 relates the precipitation changes to the global mean temperature changes. The precipitation sensitivities considering the whole tropics are only slightly higher in abrupt4×CO<sub>2</sub> than in 1pctCO<sub>2</sub>. The slope amounts to 1.8% K<sup>-1</sup> in abrupt4×CO<sub>2</sub> and 1.7% K<sup>-1</sup> in 1pctCO<sub>2</sub>, which is in the typical range of values derived from scenario runs [IPCC, 2007]. Striking differences between the experiments become apparent when the land and the ocean are treated separately, consistent with Figure 3. Over the oceans, a steady linear increase of precipitation with increasing temperature is found for both simulations. A slightly higher sensitivity is obtained for abrupt4×CO<sub>2</sub> (2.7% K<sup>-1</sup>) than for 1pctCO<sub>2</sub> (2% K<sup>-1</sup>). Over land, the picture is quite different: 1pctCO<sub>2</sub> reveals an overall increase of only 0.2% per degree temperature change. This moderate increase, however, underlies considerable variability, which leads to precipitation changes of up to 4% when temperature increases are 2 K. The abrupt4×CO<sub>2</sub> precipitation reveals negative sensitivity over land. This relates to

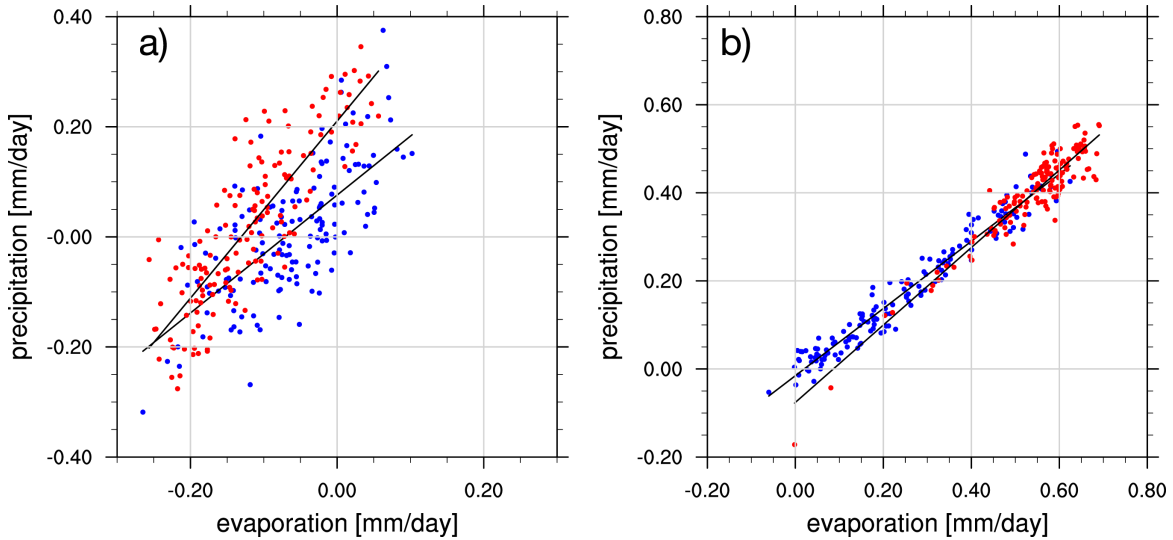


**Figure 5.** Annual mean of precipitation ( $\text{mm d}^{-1}$ ) and evaporation ( $\text{mm d}^{-1}$ ) changes with respect to piControl for 131 20-year periods for 1pctCO<sub>2</sub> (blue) and abrupt4×CO<sub>2</sub> (red) averaged over (a) the tropical land areas and (b) the tropical oceans.

the abrupt increase of precipitation in the first years of the experiment and a reduction afterward. Both experiments coincide around 5 K temperature, but it is unclear whether this is just a fortuitous occurrence. It is also unclear whether precipitation will increase or decrease beyond 5 K warming in 1pctCO<sub>2</sub>.

[17] Consideration of Figure 4 can further serve to isolate the contribution of fast versus slow processes after the method introduced by *Gregory et al.* [2004]. The intercept by 0 K indicates that over the whole tropics or the tropical ocean, the direct radiative effect of CO<sub>2</sub> (fast response) induces a precipitation reduction. This is in agreement with previous studies using different models or forcings [e.g., *Gregory and Webb*, 2008; *Dong et al.*, 2009; *Andrews and Forster*, 2010]. The result over land, with increased precipitation at the intercept, is consistent with results obtained from fixed SST experiments and is generally explained by an increased moisture convergence. This, however, cannot explain the precipitation signal obtained in several land areas in Figure 3 (see section 4). *Andrews and Forster* [2010] also noted that diagnosing the fast adjustment process occurring over land from a linear regression analysis is problematic.

[18] To further examine the precipitation change signal and especially its nonlinear relationship to temperature over land, it is useful to consider evaporation (Figure 5). The atmospheric water balance equation indicates that precipitation is balanced by evaporation, moisture convergence and change in the column storage of water vapor. Thus, to a first-order approximation precipitation tends to follow evaporation (see also section 4). This is obvious over the ocean (see Figure 5b), where precipitation increases with increasing evaporation. The regression slopes with values of 0.8 in 1pctCO<sub>2</sub> and 0.9 in abrupt4×CO<sub>2</sub> are similar. Because

the slopes are smaller than 1, humidity is increasingly advected from the tropical oceans either to the tropical land areas or the extratropics. Also, because water supply is infinite over ocean, evaporation increases with rising temperature, as long as the atmosphere is not saturated, and hence precipitation increases with increasing temperature. Over land, the picture is more complicated (see Figures 5a and 4b). Overall, precipitation changes are higher than evaporation changes, consistent with an import of additional moisture from the ocean. Like over the oceans, the slopes are positive in Figure 5a, i.e., precipitation follows evaporation. Given that with increasing temperature, evaporation continuously decreases in abrupt4×CO<sub>2</sub> (not shown), Figure 5 implies a reduction in land precipitation as the climate warms. This is consistent with Figure 4b.

### 3.3. Intraseasonal Variability

[19] The MJO is a convectively coupled circulation envelope that represents the dominant mode of intraseasonal variability in the tropics [*Madden and Julian*, 1972, 1994]. The MJO is associated with strong precipitation events over the Indian Ocean, the Warm pool, and the Eastern Equatorial Pacific. Therefore, changes in the tropical precipitation as reported above might have strong impact on the MJO. A new metric has been recently developed from an ensemble of ECHAM6 simulations by *Crueger et al.* [2012], which allows for a fast quantitative assessment of the MJO strength. The metric is based on two components, one for the mean strength of the eastward propagation and the other for the strength of the convection within the envelope.

[20] Figure 6 illustrates the sensitivity of the MJO to the temperature change for 1pctCO<sub>2</sub> and abrupt4×CO<sub>2</sub>. The sensitivities relative to piControl are different in 1pctCO<sub>2</sub> and abrupt4×CO<sub>2</sub>. 1pctCO<sub>2</sub> reveals a moderate

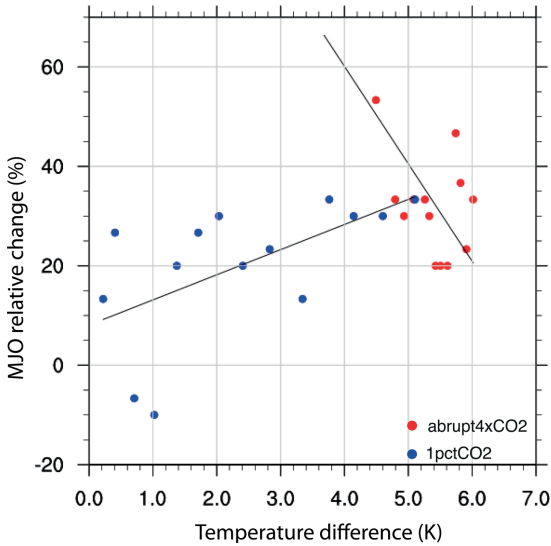


**Figure 6.** Sensitivity of MJO strength (%) with respect to global temperature change (K) for 1pctCO<sub>2</sub> (blue) and abrupt4×CO<sub>2</sub> (red). The black lines denote the linear regression lines.

strengthening of the MJO with some variability, resulting in a 30% strengthening compared to piControl and a sensitivity of 5–6% K<sup>-1</sup>. In contrast, in abrupt4×CO<sub>2</sub>, the MJO abruptly strengthens (the point by 4.5 K and 50% relative change) before settling around 30% relative change. A regression analysis yields a negative slope (−20% K<sup>-1</sup>), which is mainly caused by the first point. The abrupt MJO change at the beginning of abrupt4×CO<sub>2</sub> is due to both the abrupt increase of the rainfall signal and the strengthening of the eastward propagation, whereas a roughly continuous strengthening of eastward propagation dominates the sensitivity of 1pctCO<sub>2</sub> (not shown). It is interesting to note that the MJO sensitivities exhibit a notable similarity with those over land, but given that ECHAM6 has difficulties in reproducing precipitation over land, this result should not be overinterpreted.

### 3.4. Convection Statistics

[21] Beyond changes in mean precipitation or in its dominant mode of variability, it is important to investigate more closely changes in convective properties, such as convective cloud depth and triggering frequency, since they are tightly tied to the precipitation response. To that aim, specific years of piControl, 1pctCO<sub>2</sub>, and abrupt4×CO<sub>2</sub> were rerun with a 30-min output frequency of various quantities related to convection. This allows for a robust derivation of corresponding statistics. The analysis refers to the entire tropics except when explicitly mentioned.

[22] Figure 7 shows frequency distribution of convective cloud depth for piControl, 1pctCO<sub>2</sub>, and abrupt4×CO<sub>2</sub> and for the years 1850 and 1990. The distribution for piControl remains unchanged over time, as to be expected. Generally, 1pctCO<sub>2</sub> and abrupt4×CO<sub>2</sub> exhibit

similar distributions and similar shifts in the distributions with time. The shift happens more abruptly in abrupt4×CO<sub>2</sub> than in 1pctCO<sub>2</sub>, i.e., only by 1990 do the two curves coincide (not shown).

[23] Figure 7 indicates that more than two thirds of convective clouds have cloud depths of 1–2 km, 20% of the convective clouds have cloud depths of 3–4 km and only 10% have depths larger than 10 km in 1850. The distribution clearly shifts toward deeper convective clouds with time. The shift is from 11–15 to 12–17 km over the whole tropics (9–14 to 12–17 km over ocean and 10–15 to 12–17 km over land, not shown). This increase in depth is mainly due to increasing cloud top height, whereas the cloud base remains at constant height (not shown). Besides changes in the upper tail of the distribution, there is also an increase in the number of shallow clouds (cloud depth below 2 km) compensated by a decrease of clouds with depth around 3 km.

[24] Although deep convective clouds represent only 10% of the total convective clouds, they are responsible for 55% of the total precipitation in piControl as integrated over cloud depth higher than 10 km (Figure 8). Clouds with depths of around 5 km and less are responsible for about one third of the rainfall. Consistent with Figure 7, the shift in the deep cloud population can be recognized in 1pctCO<sub>2</sub> and abrupt4×CO<sub>2</sub>. In addition, the fraction of precipitation resulting from deep convection increases, especially in abrupt4×CO<sub>2</sub>. Deep convection accounts for two thirds of the total precipitation in abrupt4×CO<sub>2</sub> and 62% in 1pctCO<sub>2</sub> by 1990. The shift toward higher cloud depths and enhanced rainfall is already visible in the first experiment year in abrupt4×CO<sub>2</sub>, which is not the case for 1pctCO<sub>2</sub>. Concerning shallower clouds, both simulations reveal a shift toward more rain for cloud depths between 1 and 2 km, and a decrease for cloud depths between 3 and 4 km. Similar findings hold for land and ocean taken separately.

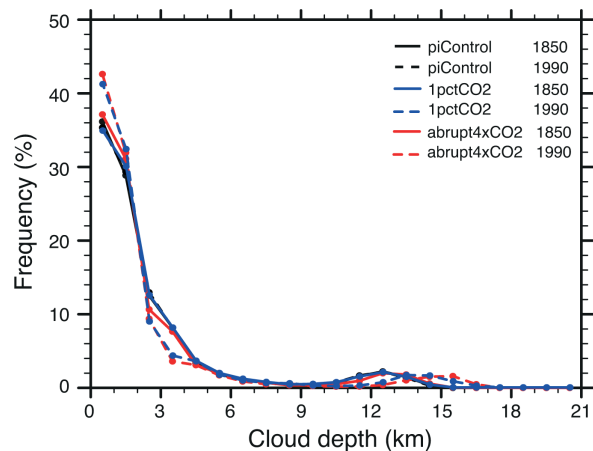


**Figure 7.** Frequency distribution (%) of cloud depth (km) for piControl (black), 1pctCO<sub>2</sub> (blue), and abrupt4×CO<sub>2</sub> (red) for the years 1850 (solid) and 1990 (dashed).

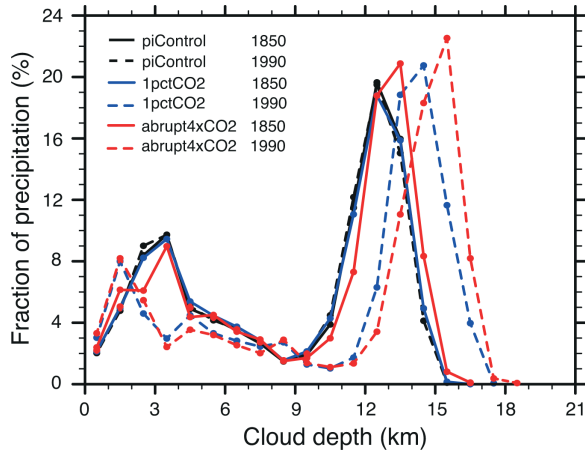


**Figure 8.** Fraction of precipitation (%) per cloud depth class for piControl (black), 1pctCO<sub>2</sub> (blue), and abrupt4×CO<sub>2</sub> (red) for the years 1850 (solid) and 1990 (dashed).

[25] Figure 9 shows the frequency distribution of cloud top temperature on a log-scale for 1850, 1990, and the three simulations. Three maxima are obvious in Figure 9. The first one, around 210 K, is associated with the deep cloud population. For all considered simulations and years the curves are similar, implying that the cloud top temperature remains constant independently of the CO<sub>2</sub> forcing (see next section). The second maximum, by 250 K in 1850, is probably associated with congestus-type clouds. The temperature at which these clouds detrain clearly shifts to warmer temperatures. Finally, the last maximum, around 290 K can be assigned to shallow clouds. Although the maximum does not shift to warmer temperatures per se, the frequency distribution broadens toward much warmer temperatures. Finally, there is no clear difference between the 1pctCO<sub>2</sub> and abrupt4×CO<sub>2</sub> curves in 1990 as well as between land and ocean (not shown).

[26] Figure 10 relates the changes in the convection statistics to the temperature changes. Only the precipitation events diagnosed as deep convection by the convection scheme are retained given that they contribute the most to precipitation. The convection scheme distinguishes between shallow, deep, and midlevel convection, meaning that the deep convective population in Figure 10 encompasses most of the clouds of Figure 8 with depths larger than 2 km. Overall, similar sensitivities are obtained in 1pctCO<sub>2</sub> and abrupt4×CO<sub>2</sub>. The different CO<sub>2</sub> forcings hardly affect the robust dependency of the convective features on temperature changes when considering the whole tropics. Precipitation intensity increases by more than 8% K<sup>-1</sup> (Figure 10a). This increase of precipitation intensity is accompanied by an increase of cloud top height at a rate of 3.8% K<sup>-1</sup> (Figure 10b). On the other hand, the deepening of the deep convective clouds with time is accompanied by a reduction of their occurrence (Figure 10c). The convective frequency is remarkably reduced in 1pctCO<sub>2</sub> and abrupt4×CO<sub>2</sub> with one third less events occurring by

5 K warming. Changes in convective frequency may be due to changes in triggering frequency and/or duration of convection. The reduction amounts to  $-5.5\% \text{ K}^{-1}$ .

[27] Similar temperature sensitivities can be found over ocean. However, over the tropical landmasses, abrupt4×CO<sub>2</sub> and 1pctCO<sub>2</sub> exhibit a distinct behavior, in agreement with section 3.2. The cloud top height increases by 3% K<sup>-1</sup> and the convective frequency decreases by 4.8% K<sup>-1</sup> both in 1pctCO<sub>2</sub> and abrupt4×CO<sub>2</sub>. The precipitation intensity nevertheless increases by 6% K<sup>-1</sup> in 1pctCO<sub>2</sub> but only by 3% K<sup>-1</sup> in abrupt4×CO<sub>2</sub>. It is evident that, in abrupt4×CO<sub>2</sub>, the increase in precipitation intensity falls short to compensate the reduced frequency, in contrast to 1pctCO<sub>2</sub>. This is consistent with precipitation amounts that generally increase in 1pctCO<sub>2</sub> but decrease in abrupt4×CO<sub>2</sub>, as previously found in Figure 4 (see also next section).

#### 4. Testing Climate Change Rules

[28] The precipitation changes depicted in the previous sections in essence result from the sensitivity of the convection scheme to changes in the environmental conditions. To better understand the results of section 3 and their robustness, it is thus useful to investigate the ability of the MPI-ESM to reproduce climate change rules. Such rules have been derived in previous studies either from physical arguments or cloud-resolving simulations with explicit convection (see Introduction). The three investigated rules are Clausius-Clapeyron scaling, the energy constraint, and the FAT hypothesis.

##### 4.1. Clausius-Clapeyron Scaling

[29] As noted in numerous studies, Clausius-Clapeyron scaling implies an approximate 7% precipitation increase per degree temperature rise. In a mean sense and in agreement with previous studies, precipitation, which increases by 1.7% K<sup>-1</sup> in 1pctCO<sub>2</sub>, does not follow the Clausius-Clapeyron equation. The obtained

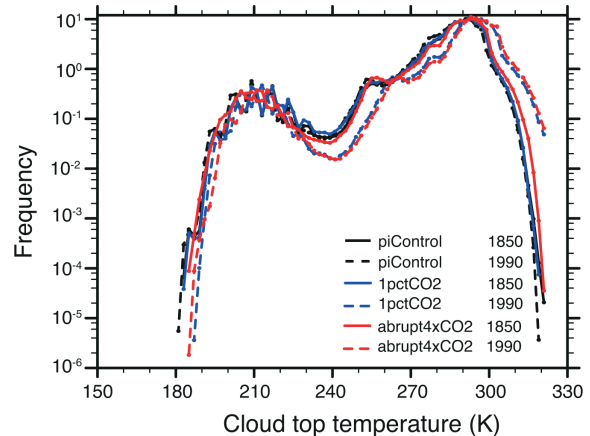


**Figure 9.** Frequency distribution (log-scale) of cloud top temperature (K) for piControl (black), 1pctCO<sub>2</sub> (blue), and abrupt4×CO<sub>2</sub> (red) for the years 1850 (solid) and 1990 (dashed).

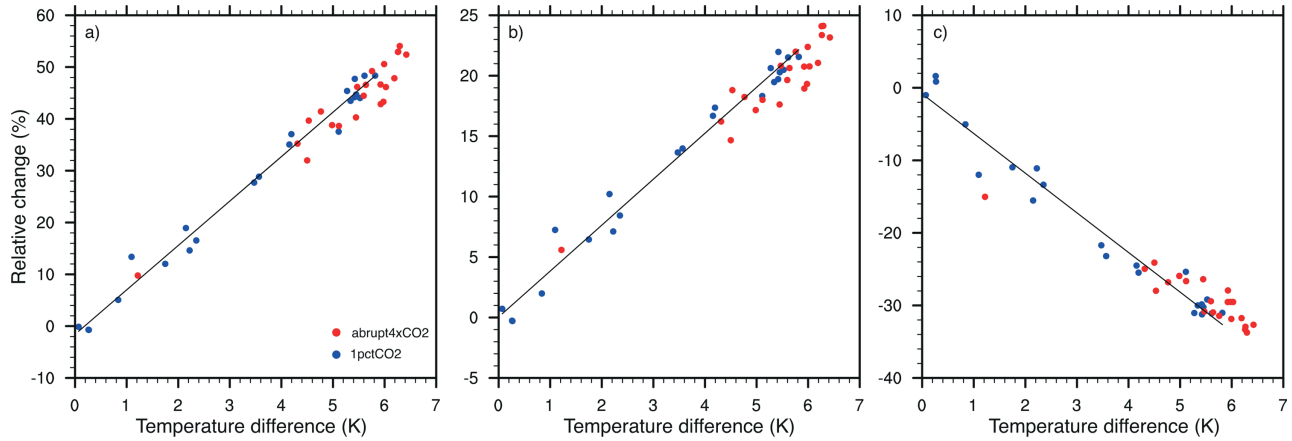


**Figure 10.** Relative change (%) in (a) precipitation intensity, (b) cloud top height, and (c) convective frequency for 1pctCO<sub>2</sub> (blue) and abrupt4×CO<sub>2</sub> (red) relative to piControl. Only deep convective events are considered. Precipitation intensity is defined as the precipitation sum divided by the number of rainy points. The dots correspond to yearly values (1850, 1851, 1870, 1871, 1890, 1891, 1910, 1911, 1930, 1931, 1950, 1951, 1970, 1971, 1990, 1991, 1992, 1993, 1994, 1995, 1996, 1997, 1998) averaged over the tropics. Black lines are the linear regression lines based on 1pctCO<sub>2</sub> with slope of 8.6% K<sup>-1</sup> in Figure 10a, 3.8% K<sup>-1</sup> in Figure 10b, and -5.5% K<sup>-1</sup> in Figure 10c.

change in precipitation intensity from deep convection, however, with its 8% increase per K, is not too far off from Clausius-Clapeyron scaling. Romps [2011] actually obtained a 7–8% K<sup>-1</sup> increase in precipitation intensity in his cloud-resolving simulations. The obtained 8% K<sup>-1</sup> increase is also consistent with changes in cloud base properties: specific humidity of cloudy points increases by approximately 7% K<sup>-1</sup> at cloud base (not shown). Therefore, over the whole tropics or the ocean, the convection scheme is able to reproduce results from cloud-resolving models and physical expectations. This is not true over land, where even the change in precipitation intensity does not follow Clausius-Clapeyron relation.

#### 4.2. Energy Constraint

[30] Whereas mean precipitation does not follow Clausius-Clapeyron scaling, it has been shown to be constrained on a large scale by the available energy [e.g., Allen and Ingram, 2002; Held and Soden, 2006]. This remains true in the MPI-ESM, where both mean precipitation and the latent heat flux increase by 1.7% K<sup>-1</sup> in 1pctCO<sub>2</sub>. Reconciling an increase in precipitation intensity following the Clausius-Clapeyron equation and a change in mean precipitation slaved to the available energy implies a decrease in precipitation frequency, as argued for instance in Trenberth et al. [2003]. This fits with the -5.5% K<sup>-1</sup> frequency reduction predicted by the convection scheme or with Romps’s [2011] results.

[31] The precipitation changes obtained in distinct regions as well as over land versus ocean are more interesting to consider since precipitation is not constrained by the energy budget on a regional scale. Although precipitation does not need to compensate evaporation, changes in precipitation are still highly correlated to changes in evaporation, as indicated in section 3.2 and Figure 5. This is not surprising given that mean precipi-

tation is highly correlated to mean evaporation, i.e., the cloud base mass flux predicted by the convection scheme tends to track the latent heat flux.

[32] The fact that precipitation changes are not well constrained except for the convection scheme keeping track of the latent heat flux becomes more apparent when comparing the results of the 1pctCO<sub>2</sub> and abrupt4×CO<sub>2</sub> experiments over land. Evaporation is determined by the available energy and by land surface processes, such as plant physiological effects or soil moisture availability. Previous studies have indicated that precipitation is strongly linked to land surface processes over Amazonia, the Sahel region, Central America, and parts of India [see e.g., Figure 1 in Koster et al., 2004]. This may be seen as consistent with a strong increase in evaporation in abrupt4×CO<sub>2</sub> in the first year followed by decreasing values, expressing an ongoing drying of the soil. Recent studies have also suggested that under strong CO<sub>2</sub> concentration, plants close their stomata, which reduce transpiration and at least amplify the warming over land [e.g., Joshi et al., 2008; Cao et al., 2009]. This may further contribute to the reduction in evaporation and thus to the different sensitivities displayed by abrupt4×CO<sub>2</sub> and 1pctCO<sub>2</sub>.

[33] Along similar arguments, the strongest precipitation decreases are expected where temperatures raise the most. This is actually found for tropical South America, which shows the highest temperature changes among the tropical land areas and a strong precipitation reduction. Also, the temperature increase over tropical Asia is smallest compared with the other land areas and precipitation does not decrease, but even increases. Since convection schemes have some limitations in representing interactions between land processes and precipitation [see Hohenegger et al., 2009], the precipitation changes obtained over land cannot be constrained and are not robust.

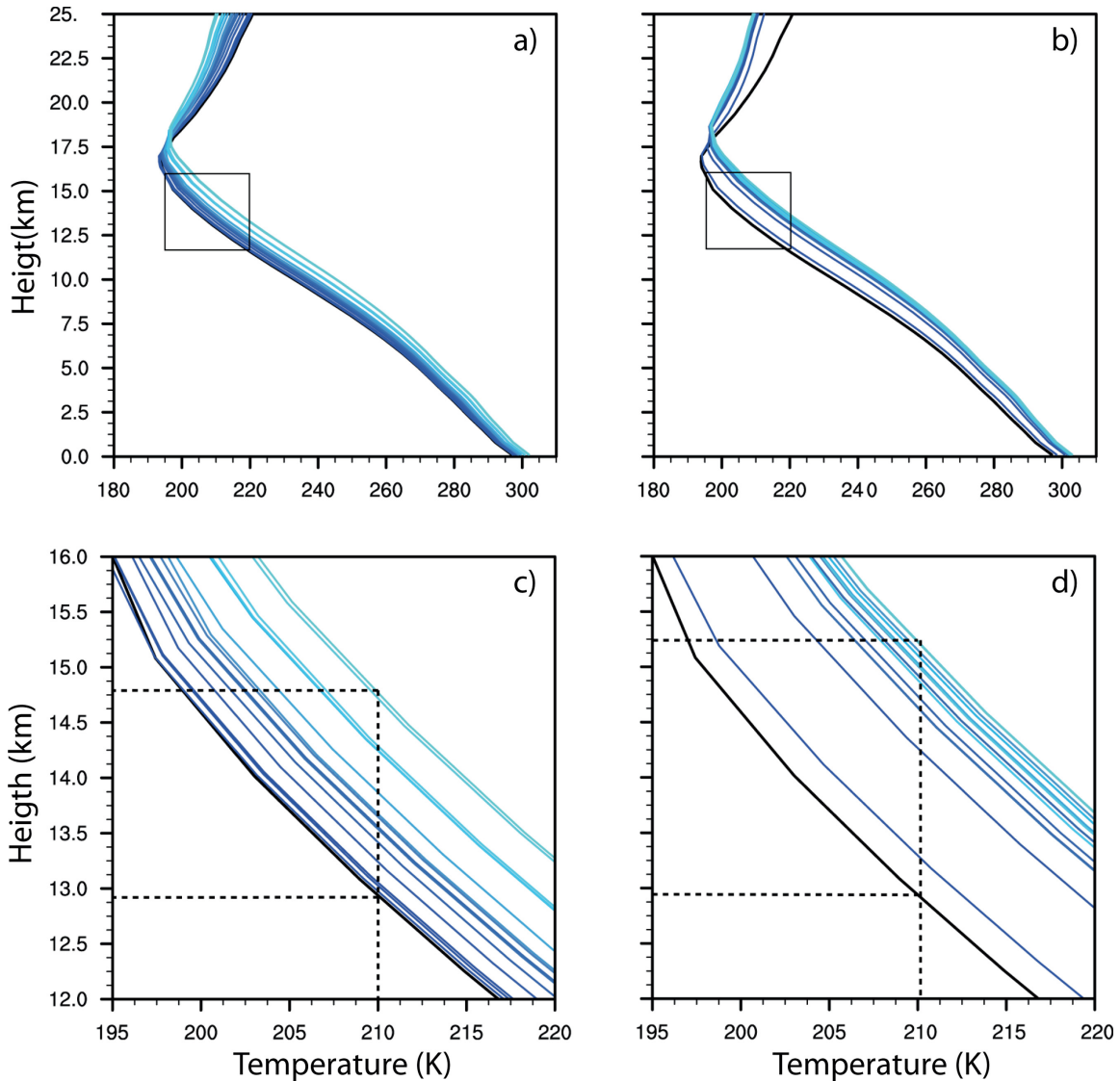


**Figure 11.** Vertical temperature profiles for 1850, 1860, ..., 1990 for (a, c) 1pctCO<sub>2</sub> and (b, d) abrupt4×CO<sub>2</sub> averaged over the tropics. Figures 11c and 11d represent a magnification of the square drawn in Figures 11a and 11b. Blue color gets lighter in the course of time. The vertical dashed line represents 210 K, the deep convective cloud top temperature, whereas the horizontal dashed lines indicate the corresponding altitude for the year 1850 (black curve) and 1990 (last blue curve).

#### 4.3. Fixed-Anvil Temperature

[34] The temperature at which tropical convective anvils detrain is an important constraint on tropical cloud-climate. The analysis of the convection statistics in section 3.4 reveals that the cloud top temperature of the deep convective clouds remains constant (Figure 9). Thus, the MPI-ESM and its convection scheme support the FAT hypothesis, although large-scale circulation might have affected it, as suggested by *Kuang and Hartmann* [2007]. Assuming FAT, the change in cloud top height can be estimated directly from the vertical temperature profile, rather than from the convection statistics. This is because temperatures in the tropics are

dynamically constrained to be very uniform above the boundary layer, i.e., the anvil and the clear sky temperatures are similar [*Held and Soden*, 2006]. Thus, the tropical mean temperature profile also represents the temperature of the anvils. Vertical profiles of mean tropical temperature are displayed in Figure 11 for 1pctCO<sub>2</sub>, abrupt4×CO<sub>2</sub>, and different years. Figure 11 reveals an increase of the tropopause height with time, continuous for 1pctCO<sub>2</sub> and abrupt for abrupt4×CO<sub>2</sub>. Apparent is also that the surface temperature increases less than the temperature at higher altitudes up to the tropopause, consistent with a temperature profile shifting to a next moist adiabat. Figures 11c and 11d zoom

in the temperature profiles around 210 K, i.e., the temperature of deep convective cloud top height in the simulations (Figure 9). Assuming a constant cloud top height temperature, Figure 11 yields an increase in cloud top height of approximately 1.9 km for 1pctCO<sub>2</sub> and 2.3 km for abrupt4×CO<sub>2</sub>. This implies a cloud top height sensitivity of 3% K<sup>-1</sup> for 1pctCO<sub>2</sub> and 4% K<sup>-1</sup> for abrupt4×CO<sub>2</sub>. This agrees well with the 3.8% K<sup>-1</sup> obtained in section 3.4 based on the convection statistics. Stated in other words, the convection scheme is able to reproduce the FAT hypothesis, which constrains the simulated upper tropospheric temperature profile.

## 5. Conclusions

[35] In this study, the response of tropical precipitation and convection to idealized CO<sub>2</sub> forcings has been examined using the latest and fully coupled release of the Max Planck Institute Earth system model (MPI-ESM). Sensitivity to an abrupt CO<sub>2</sub> increase of 4 times its preindustrial concentration and to a transient CO<sub>2</sub> increase of 1% per year has been examined. With the exceptions of tropical continental precipitation and MJO strength, the MPI-ESM shows a robust response to climate change, which is not dependent on the CO<sub>2</sub> pathway. Over land, in contrast, abrupt versus transient simulations yield a similar geographical distribution of the precipitation change signal but supports a different time evolution.

[36] Averaged over the tropics, precipitation increases by 1.7% K<sup>-1</sup>. Deep convective events are more intense (8% K<sup>-1</sup>), less frequent (-5.5% K<sup>-1</sup>), and deeper (3.8% K<sup>-1</sup> change in cloud top height). The cloud top temperature of deep clouds remains constant with time, whereas cumulus congestus and shallow clouds warm as the climate warms. These characteristics are as to be expected from physical argumentation and/or cloud-resolving models using explicit convection. Therefore, on a large scale, the convection scheme seems to behave in a robust way. This also means that, knowing the cloud top temperature in present-day climate allows “predicting” the cloud top height in future climate (with the FAT hypothesis), the changed precipitation intensity and cloud base properties (with Clausius-Clapeyron scaling), the changed precipitation frequency (energy constraint) and the profile of temperature (via a moist adiabat). This remains valid over the oceans but breaks down over land except for the fact that the convection scheme (and precipitation) tends to track evaporation. Given that evaporation is tied to land surface processes, which seem to respond differently to a transient or abrupt CO<sub>2</sub> forcing and whose interactions with convection are generally not well represented in climate models, no strong constraint exists for the convection scheme over land.

[37] **Acknowledgments.** This research was made possible through the support of the Max Planck Society for the Advancement of Science and the German Climate Computing Center (DKRZ), Hamburg, and of the Danish Ministry of Climate, Energy and Building, Copenhagen, Denmark. Some of this research has received funding from the

European Union, Seventh Framework Programme (FP7/2007-2013) under grant agreement 244067.

## References

- Allen, M. R., and W. J. Ingram (2002), Constraints on future changes in climate and the hydrological cycle, *Nature*, *419*, 224–232.
- Andrews, T., and P. M. Forster (2010), The transient response of global-mean precipitation to increasing carbon dioxide, *Environ. Res. Lett.*, *5*, 025212.
- Bony, S., and J.-L. Dufresne (2005), Marine boundary layer clouds at the heart of tropical feedback uncertainties in climate models, *Geophys. Res. Lett.*, *32*, L20806, doi:10.1029/2005GL023851.
- Cao L, G. Bala, K. Caldeira, R. Nemani, and G. Ban-Weiss (2009), Climate response to physiological forcing of carbon dioxide simulated by the coupled Community Atmosphere Model (CAM3.1) and Community Land Model (CLM3.0), *Geophys. Res. Lett.*, *36*, L10402, doi: 10.1029/2009GL037724.
- Crueger, T., B. Stevens, and R. Brokopf (2012) The Madden-Julian oscillation in ECHAM6 and the introduction of a MJO metric, *J. Clim.*, doi: 10.1175/JCLI-D-12-00413.1.
- Dong, B., J. M. Gregory, and R. T. Sutton (2009) Understanding land-sea warming contrast in response to increasing greenhouse gases, Part I: transient adjustment. *J. Clim.*, *22*, 3079–3097.
- Gregory, J., and M. Webb (2008), Tropospheric adjustment induces a cloud component in CO<sub>2</sub> forcing. *J. Clim.*, *21*, 58–71.
- Gregory, J., W. J. Ingram, M. A. Palmer, G. S. Jones, P. A. Stott, R. B. Thorpe, J. A. Lowe, T. C. Johns and K. D. Williams (2004), A new method for diagnosing radiative forcing and climate sensitivity, *Geophys. Res. Lett.*, *31*, L03205, doi:10.1029/2003GL018747.
- Hartmann, D. L., and K. Larson (2002), An important constraint on tropical cloud — Climate feedback, *Geophys. Res. Lett.*, *29*(20), 1951, doi:10.1029/2002GL015835.
- Held, I. M., and B. J. Soden (2006), Robust responses of the hydrological cycle to global warming, *J. Clim.*, *19*, 5686–5699.
- Hohenegger, C., P. Brockhaus, C. S. Bretherton, and C. Schär (2009), The soil moisture-precipitation feedback in simulations with explicit and parameterized convection, *J. Clim.*, *22*, 5003–5020.
- Ilyina, T., et al. (2013), The global ocean biogeochemistry model HAMOCC: Model architecture and performance as component of the MPI Earth system model in different CMIP5 experimental realizations, *J. Adv. Model. Earth Syst.*, in press.
- Intergovernmental Panel on Climate Change (IPCC) (2007), *Climate Change 2007—The Physical Science Basis: Contribution of Working Group I to the Fourth Assessment Report of the Intergovernmental Panel on Climate Change*, edited by S. Solomon et al., Cambridge Univ. Press, Cambridge, U. K., 747–845.
- Johns, T. C., et al. (2011), Climate change under aggressive mitigation: the ENSEMBLES multi-model experiment, *Clim. Dyn.*, *37*, 1975–2003.
- Joshi, M., J. Gregory, M. Webb, D. Sexton, and T. Johns (2008), Mechanisms for the land/sea warming contrast exhibited by simulations of climate change, *Clim. Dyn.*, *30*, 455–465.
- Knutson, T. R., and S. Manabe (1995), Time-mean response over the Tropical Pacific to increased CO<sub>2</sub> in a coupled ocean-atmosphere model, *J. Clim.*, *8*, 2181–2199.
- Koster, R. D., et al. (2004), Regions of strong coupling between soil moisture and precipitation, *Science*, *305*, 1138–1140.
- Kuang, Z., and D. L. Hartmann (2007), Testing the fixed anvil temperature hypothesis in a cloud-resolving model, *J. Clim.*, *20*, 2051–2057.
- Madden, R., and P. Julian (1972), Description of global-scale circulation cells in the tropics with a 40–50-day period, *J. Atmos. Sci.*, *29*, 1109–1123.
- Madden, R., and P. Julian (1994), Observations of the 40–50-day tropical oscillation: A review, *Mon. Weather Rev.*, *112*, 814–837.
- Nordeng, T. E., (1994), Extended versions of the convective parameterization scheme at ECMWF and their impact on the mean and transient activity of the model in the tropics, Tech. Memo. 206, Eur. Centre for Medium-Range Weather Forecasts, Reading, U. K.
- Romps, D. M. (2011), Response of tropical precipitation to global warming, *J. Atmos. Sci.*, *68*, 123–138.
- Satoh, M., S.-I. Iga, H. Tomita, Y. Tsumura, and A. T. Noda (2012), Response of upper clouds in global warming experiments obtained

- using a global nonhydrostatic model with explicit cloud processes, *J. Clim.*, *25*, 2178–2199.
- Stevens, B., et al. (2013), The atmospheric component of the MPI-M earth system model: ECHAM6, *J. Adv. Model. Earth Syst.*, in press.
- Sutton, R. T., B. W. Dong, and J. M. Gregory (2007), Land/sea warming ratio in response to climate change: IPCC AR4 model results and comparison with observations, *Geophys. Res. Lett.*, *34*, L02701, doi:10.1029/2006GL028164.
- Taylor, K. E., R. J. Stouffer, and G. A. Meehl (2012), An overview of CMIP5 and the experiment design, *Bull. Am. Meteorol. Soc.*, *93*, 485–498.
- Tiedtke, M. (1989), A comprehensive mass flux scheme for cumulus parameterization in large-scale models, *Mon. Weather Rev.*, *117*, 1779–1800.
- Trenberth K. E., A. Dai, R. M. Rasmussen, and D. B. Parsons (2003), The changing character of precipitation, *Bull. Am. Meteorol. Soc.*, *84*, 1205–1217.
- Wright, J. S., A. Sobel, and J. Galewsky (2010), Diagnosis of zonal mean relative humidity changes in a warmer climate, *J. Clim.*, *23*, 4556–4569.
- Yang, F. L., et al. (2003), Intensity of hydrological cycles in warmer climates, *J. Clim.*, *16*, 2419–2423.
- Zhang, C. (2005), Madden-Julian oscillation, *Rev. Geophys.*, *43*, 1–36.

---

Corresponding author: T. Crueger, Max Planck Institute for Meteorology, Bundesstrasse 53, D-20146 Hamburg, Germany. (traute.crueger@zmaw.de)